Reynolds number effects in pipe flow turbulence of generalized Newtonian fluids

J. Singh, M. Rudman, and H. M. Blackburn

Phys. Rev. Fluids **3**, 094607 — Published 28 September 2018

DOI: 10.1103/PhysRevFluids.3.094607

Reynolds number effects in pipe flow turbulence of generalised Newtonian fluids

J. Singh,[1, a)] M. Rudman,[1] and H. M. Blackburn[1]
Department of Mechanical and Aerospace Engineering, Monash University, Vic 3800, Australia

(Dated: 13 September 2018)

The turbulent pipe flow of inelastic shear thinning fluids has many practical applications, however there is a deficit in understanding of how shear thinning rheology modifies turbulence structure in the near-wall boundary layer (affecting shear stress and pressure drop) and in the core (affecting mixing). While previous direct numerical simulation studies have examined the effect of shear-thinning rheology at low Reynolds number ($Re_{\tau,max} = 323$), the way in which these effects vary with Re_τ was unknown. In particular, from earlier work it was unclear if inner-scaled mean axial velocity profiles for Newtonian and shear-thinning fluids could collapse to a common curve with increasing Reynolds number. Via direct numerical simulations of Newtonian and one shear-thinning rheology for friction Reynolds number $Re_\tau = 323 - 750$ ($Re_G = 10\,000 - 28\,000$), the current study investigates how increasing Reynolds number modifies turbulent pipe flow of a power-law fluid with particular focus on the boundary layer profiles. The results show that the inner-scaled mean axial velocity profiles for Newtonian and shear-thinning fluids can not collapse to a common curve with increasing Reynolds number, which is consistent with predictions from the Dodge & Metzner correlation. In inner-scaled coordinates, mean viscosity profiles are shown for the first time to become independent of Reynolds number except close to the pipe centre. The contribution of viscosity fluctuations in the mean shear budget and in the mean flow and turbulence kinetic energy budget remains small at all Re. Both increasing Reynolds number and shear thinning influence the turbulence kinetic energy budget near the wall, however, the region where shear-thinning is important is much wider than the region where increasing Reynolds number influences the results. The persistence of shear-thinning effects on turbulence modification in pipe flow requires consideration in the development of suitable turbulence models for such fluids. The current results suggest that the effect of shear-thinning rheology in turbulence models can be captured via a Reynolds-number-independent mean viscosity model in the inner region.

I. INTRODUCTION

Many fluids in industry and nature exhibit a non-uniform viscosity which can depend on several parameters such as shear rate, shear history and fluid viscoelasticity. These fluids are called non-Newtonian fluids. Generalised Newtonian (GN) fluids is a subclass of non-Newtonian fluids for which the shear stress tensor $\boldsymbol{\tau}$ can be written as:

$$\boldsymbol{\tau} = \rho\nu(\dot{\gamma})\boldsymbol{s}. \tag{1}$$

Here shear rate $\dot{\gamma} = (2\boldsymbol{s} : \boldsymbol{s})^{1/2}$ is the second invariant of the strain rate tensor $\boldsymbol{s} = [(\boldsymbol{\nabla v}) + (\boldsymbol{\nabla v})^T]/2$ where T represents matrix transpose, $\boldsymbol{v}$ is the velocity, ρ is fluid density and ν is fluid kinematic viscosity (also called the effective viscosity). The GN assumption asserts an instantaneous response of the fluid to the applied shear stress. GN fluids can be shear-thinning or shear-thickening depending on whether their viscosity decreases or increases with increasing shear rate. Modern paints, mining slurries, tomato ketchup, human blood are examples of GN fluids[1].

Viscosity of GN fluids is often expressed via a mathematical equation called a rheology model which defines the function $\nu(\dot{\gamma})$. The power-law (PL) rheology model is one such rheology model which is widely used for shear-thinning GN fluids (here onwards referred to as shear-thinning fluids). It defines the fluid kinematic viscosity as:

$$\nu = \rho^{-1} K \dot{\gamma}^{n-1}, \tag{2}$$

where fluid consistency K and flow index n are constants. For $0 < n < 1$, the PL rheology model gives shear-thinning behaviour and for $n = 1$ it reduces to a Newtonian rheology (uniform viscosity). We note that the PL rheology model is one of the many rheology models available for GN fluids, however, if an appropriate range of shear rate is covered in rheology characterisation, the choice of the rheology model does not significantly affect the turbulent flow predictions[2]. Although PL rheology model shows unrealistic viscosities at shear rates close to zero, it is not a concern for turbulent flow simulations where viscosity at such low shear rates are irrelevant[2].

Turbulent pipe flow of GN fluids has gained much attention due to its industrial relevance. Experimental studies, however, were focused mainly on devising a correlation for the turbulent Fanning friction factor $f = 2\tau_w/\rho U_b^2$, where $\tau_w = (D/4)\partial P/\partial z$ is the mean wall shear stress, $\partial P/\partial z$ is the mean axial pressure gradient, D is the pipe diameter and U_b is the bulk velocity (flow rate per unit area). One such early study is by Metzner and Reed[3]. The non-uniform viscosity of GN

a) Electronic mail: jagmohan.singh@monash.edu

fluids makes the choice of viscosity scale in the conventional Reynolds number definition $Re = U_b D/\nu$ ambiguous. By collapsing the laminar friction factor curve of PL and Newtonian fluids, Metzner & Reed proposed the following definition which is now called Metzner–Reed Reynolds number.

$$Re_{MR} = \frac{8\rho U_b^{2-n} D^n}{K(6+2/n)^n}. \tag{3}$$

For a Newtonian fluid ($n = 1$) Re_{MR} reduces to Re. Metzner & Reed reported a decrease in the turbulent friction factor for a fixed Re_{MR} and delay in transition to turbulence to a higher Re_{MR} with shear thinning. The friction factor measurements in laminar flows agreed well with the theoretical curve $f = 16/Re_{MR}$. In contrast, their turbulent flow measurements were scattered, which they suggested was due to the lack of fully developed turbulence at those Reynolds numbers. Metzner & Reed also proposed a turbulent friction factor correlation, however, the constants in the correlation were determined empirically using only three to four data points which made the correlation unreliable. Since Metzner & Reed several other turbulent friction factor correlations have been proposed for GN fluids[4], however for PL fluids, the Dodge & Metzner correlation[5] which is given as:

$$\frac{1}{\sqrt{f}} = \frac{4.0}{(n)^{0.75}} \log_{10}[Re_{MR}(f)^{1-n/2}] - \frac{0.4}{(n)^{1.2}} \tag{4}$$

has been found to agree the best with experimental measurements[6].

It is worthwhile mentioning here that the Metzner–Reed Reynolds number is not the only Reynolds number definition available for GN fluids. An alternate definition called the generalised Reynolds number (Re_G) defined as:

$$Re_G = U_b D/\nu_{\mathrm{w}}. \tag{5}$$

is also widely used[7–11] for GN fluids. This Reynolds number definition uses the nominal wall viscosity ν_w for the viscosity scale as proposed by Bogue and Metzner[7]. The nominal wall viscosity ν_w is the fluid viscosity at the wall shear rate in a laminar pipe flow and for PL fluids, it is given as:

$$\nu_w = \rho^{-1} K^{1/n} \tau_w^{1-1/n}. \tag{6}$$

The nominal viscosity ν_w should not be confused with the mean wall viscosity $\bar{\nu}_w$ which is obtained posteriori in simulations as a time-averaged quantity. It is almost impossible to determine $\bar{\nu}_w$ experimentally due to difficulties involved in accurately resolving the wall velocity gradients in experiments. In contrast, the nominal wall viscosity ν_w can be easily determined in experiments from the measurements of the mean axial pressure gradient and rheology. For turbulent pipe flow of shear-thinning fluids, Singh, Rudman, and Blackburn[8] showed via numerical simulation that $\bar{\nu}_w$ was only slightly higher ($\approx 2\%$) than ν_w at $Re_G \approx 11\,000$.

As mentioned earlier, most experimental studies of turbulent pipe flow of GN fluids were focused on the friction factor measurements and lacked statistical data of velocity fluctuations and Reynolds shear stresses. Park *et al.*[12] was the first study where such measurements were reported, however, only for weakly turbulent flows ($Re_G \leq 3500$). They recorded an increase in the axial velocity fluctuations and decrease in the tangential velocity fluctuations with shear thinning. Similar findings were reported by Pinho and Whitelaw[13] for a much higher Reynolds number $Re_G \approx 111\,000$. However, the fluids Pinho & Whitelaw used (Carboxymethyl cellulose solutions) are known to exhibit some visco-elasticity[5] and therefore, were not pure GN fluids.

Direct numerical simulations (DNS) is a powerful tool to investigate turbulent flows. DNS captures all dynamically relevant length scales and once validated, can be reliably used to obtain a detailed picture of the flow. DNS of Newtonian fluids does not require any empirical correlation or model, however in case of GN fluids, it relies on the rheology model $\nu(\dot{\gamma})$ for estimating viscosity. Since the rheology model and its parameters are determined via regression from the experimental data, any error introduced in the rheology characterisation can significantly affect the accuracy of the DNS predictions for GN fluids. Recently we showed that the high shear rate data is the most important factor to get a good agreement between DNS and experiments[2]. In contrast, the errors introduced in the rheology characterisation at low shear rates such as those found near the pipe centre had no noticeable effect on the DNS predictions.

DNS has been successfully used to investigate the effect of GN rheology on turbulent flow[2,8–11,14]. Similar to experiments[12,13], DNS has also shown increased turbulent anisotropy in the flow with shear thinning[8,9,11], which is hypothesised to be a result of reduced turbulent energy transfer from the axial component to the transverse ones[11]. Axial velocity streaks which are the imprints of axial vortical structures have been found to run longer and become wider with shear thinning[8,9]. We recently analysed the mean flow and turbulent kinetic energy budgets in pipe flow for PL fluids at a fixed Reynolds number of $Re_G \approx 11\,000$ and found the shear-thinning effect on the energy budgets to be confined mostly near the wall[8]. We confirmed these findings in a separate study[15] where we compared the results of PL and modified PL rheology models (PL rheology near the wall and a Newtonian rheology away from the wall). Modifying the PL rheology model away from the wall did not affect the profiles of mean axial velocity and Reynolds shear stresses.

With increasing Reynolds number, the viscous region in a turbulent pipe flow becomes smaller (in outer units) and thus, inertial effects become more dominant compared to viscous effects. Therefore, one might expect the effect of shear-thinning rheology on turbulence statistics to disappear at large Reynolds number. However, by analysing the DNS of turbulent pipe flow of Newtonian and PL fluids for $10\,000 < Re_G < 28\,000$, the current study shows that this is not true. The results show noticeable shear-thinning effects on the turbulence statistics in the Reynolds number range considered here with no evidence that these effects will disappear ever for very high Reynolds numbers. The mean axial velocity profiles of PL fluids becomes Reynolds number invariant in the inner layer and converge to a profile with a larger shift compared to the Newtonian log-law profile. In addition to these new results, the statistics of mean flow and turbulent kinetic energy budgets are presented, which will be useful for the development and validation of RANS and LES models for GN fluids.

II. METHODOLOGY

A. Numerical method and non-dimensional variables

The numerical method used here is identical to that used in our earlier studies[8–10]. Here, we briefly review the simulation methodology. For an incompressible fluid with a spatially varying viscosity, the conservation of mass and momentum equations can be written as:

$$\partial \boldsymbol{v}/\partial t+\boldsymbol{v}\cdot\boldsymbol{\nabla}\boldsymbol{v} = \rho^{-1}\left(-\boldsymbol{\nabla}p+\boldsymbol{\nabla}\cdot\boldsymbol{\tau}+\rho\boldsymbol{g}\right), \text{with } \boldsymbol{\nabla}\cdot\boldsymbol{v}=0 \quad (7)$$

where $\boldsymbol{v}$ is the velocity vector, p is the static pressure, $\boldsymbol{\tau}$ is the stress tensor and $\rho\boldsymbol{g}$ is body force. In the simulations, there is no mean axial pressure gradient and the flow is driven by the body force. For ease of notation, we divide p, $\boldsymbol{\tau}$ and $\rho\boldsymbol{g}$ in Eq. 7 by the constant fluid density ρ, but refer to them as pressure, stress and body force respectively. These governing equations are solved using a nodal spectral element-Fourier DNS code. The modified shear stress tensor, $\boldsymbol{\tau}/\rho$, is modelled via the GN assumption (Eq. 1) and the fluid viscosity, $\nu(\dot{\gamma})$, is modelled via the PL rheology model (Eq. 2). Note that the PL rheology model gives an infinite viscosity at zero shear rate, however, shear rates close to zero are unlikely to occur under turbulent flow conditions. Therefore, the infinite viscosity of the PL rheology model at zero shear rate is not an issue for modelling turbulent flow of shear-thinning fluids and can be avoided safely by techniques such as using a bi-viscosity model[16]. The governing equations are solved in Cartesian coordinates where the pipe cross section ($x-y$ plane) is discretized using spectral elements as shown in Fig. 1, while Fourier expansion is used in the axial (z) direction which is thus periodic. Results are later transformed for presentation in cylindrical coordinates with subscripts r and θ representing the quantities in the radial and the azimuthal directions. For more details of the simulation code we refer the reader to Rudman *et al.*[9], Rudman and Blackburn[10], Blackburn and Sherwin[17].

For much of the analysis presented here, the results are expressed in wall units using friction velocity $u^* = (\tau_w/\rho)^{1/2}$ for velocity scale, ν_w for the viscosity scale and ν_w/u^* for the length scale. Thus, the non-dimensional distance from the wall is given as $y^+ = (R-r)/(\nu_w/u^*)$ where r is the radial distance from the pipe centre and R is pipe radius. The non-dimensional mean axial velocity and mean viscosity are expressed as $U_z^+ = U_z/u^*$ and $\nu^+ = \bar{\nu}/\nu_w$. Turbulence intensities are expressed in wall units as $u_i'^+ = (\overline{u_i'^2})^{1/2}/u^*$. Shear rate is normalised by u^{*2}/ν_w, stress terms by ρu^{*2} and the energy budget terms by $(u^*)^4/\nu_w$. Therefore, using the scaling The y^+ definition is also referred to as the distance from the wall in inner coordinates since the distance is scaled by viscous units. In outer coordinates, the non-dimensional distance from the wall is expressed as y/R.

(*a*)

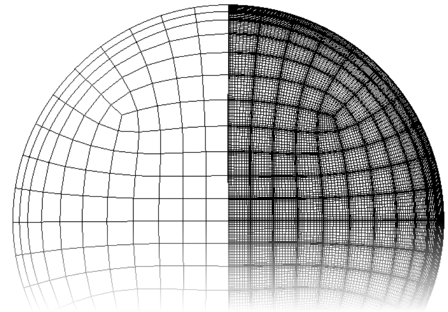

(*b*)

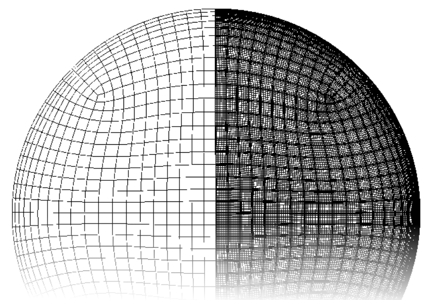

FIG. 1. Detail of spectral element meshes used to discretise pipe cross-section. The mesh in (a) has 300 spectral elements with 11th-order element interpolation functions and was used for $Re_\tau = 323$. The mesh in (b) has 1188 spectral elements and was used for $Re_\tau = 500$ with 8th-order interpolation function and for $Re_\tau = 750$, 10th-order interpolation functions were used. In each panel, spectral element boundaries are shown at left and collocation points at right.

B. Simulation parameters

Simulations are run for flow indices $n = 0.6$ and $n = 1.0$ (Newtonian). For PL fluid, the flow index $n = 0.6$ is chosen here because of its prevalence in industrial fluids. Newtonian simulations are run so that a direct comparison between Newtonian and shear-thinning fluids could be made. Because bulk velocity U_b is a predicted or measured quantity, the bulk velocity dependent Reynolds numbers Re_{MR} or Re_G can not be determined a priori. Therefore, we define a friction Reynolds number as:

$$Re_\tau = u^* R/\nu_w \tag{8}$$

This definition of Re_τ is consistent with the Newtonian definition with ν_w used for the viscosity scale. An advantage of this definition is that for a given mean wall shear stress τ_w i.e. body force and rheology, Re_τ can be calculated a priori and can be fixed in simulations with predefined rheologies.

Simulations were run for three friction Reynolds numbers $Re_\tau = 323$, 500 and 750, the parameters for which are supplied in Table I. The non-dimensional body force $gR/u^{*2} = 2$ and the nominal wall viscosity $\nu_w = 1/Re_\tau$ are set in simulations. It is important to note the implications of fixing Re_τ for Re_{MR} and Re_G. The friction Reynolds number Re_τ is related to Re_G and Re_{MR} via the friction factor f as:

$$Re_G = Re_\tau/(f/8)^{1/2},$$
$$Re_{MR} = \frac{Re_\tau^n 2^{4-n/2}}{[3+1/n]^n f^{1-n/2}}. \tag{9}$$

Due to drag reduction produced by shear-thinning (lower f), slightly higher values of Re_G are expected for PL fluid compared to Newtonian fluid for a fixed Re_τ (Table I). The relationship between Re_τ and Re_{MR} is complex. Table I shows the lower fluid consistency K and Metzner–Reed Reynolds number Re_{MR} for PL fluid compared to Newtonian fluid and only at $Re_\tau = 750$ is Re_{MR} for PL fluid close to the Newtonian value at $Re_\tau = 323$ (10 450 vs. 10 322). However, as will be seen later in Figs. 6 (a) and 7 (c), these two flows ($n = 1.0$, $Re_\tau = 323$ and $n = 0.6$, $Re_\tau = 750$) differ from each other. This suggests that Re_{MR} may not be appropriate for characterising turbulent pipe flow of different n. The normalised bulk velocity U_b/u^* is higher for the PL fluid than Newtonian fluid, which is due to the turbulent drag reduction by shear thinning[8]. The ratio of Newtonian and non-Newtonian friction factors slightly decreases with increasing Re_τ; this is further discussed in Section III B along-with the results of the friction factor.

The viscosity rheograms are plotted in wall units on linear-linear and log-log axes in Fig. 2. These plots are only dependent on the fluid rheology, not the flow regime and therefore, are identical for different Re_τ. As set, both PL and Newtonian fluids show the same viscosity at the nominal shear rate $\dot\gamma = \dot\gamma_w$ ($\dot\gamma^+ = 1$). Near the wall where shear rates $\dot\gamma^+ > 1$ are common[2] and there PL fluid shows smaller viscosity than Newtonian fluid. However, the PL fluid viscosity is higher than the Newtonian fluid away from the wall ($\dot\gamma^+ < 1$).

Re_τ	n	$K/(\rho u^{*2-n} R^n)$	Re_G	Re_{MR}	U_b/u^*	f_N/f_{NN}
323	1.0	3.0870×10^{-3}	10 322	10 322	15.93	-
	0.6	31.181×10^{-3}	11 189	5498	17.28	1.176
500	1.0	1.9996×10^{-3}	17 260	17 260	17.04	–
	0.6	24.0201×10^{-3}	18 471	7836	18.47	1.174
750	1.0	1.3333×10^{-3}	27 000	27 000	18.04	–
	0.6	18.8348×10^{-3}	28 600	10 450	19.47	1.165

TABLE I. Simulation parameters for Newtonian and PL ($n = 0.6$) liquids for different Re_τ. The non-dimensional body force gR/u^{*2} is 2 and the nominal wall viscosity is $1/Re_\tau$.

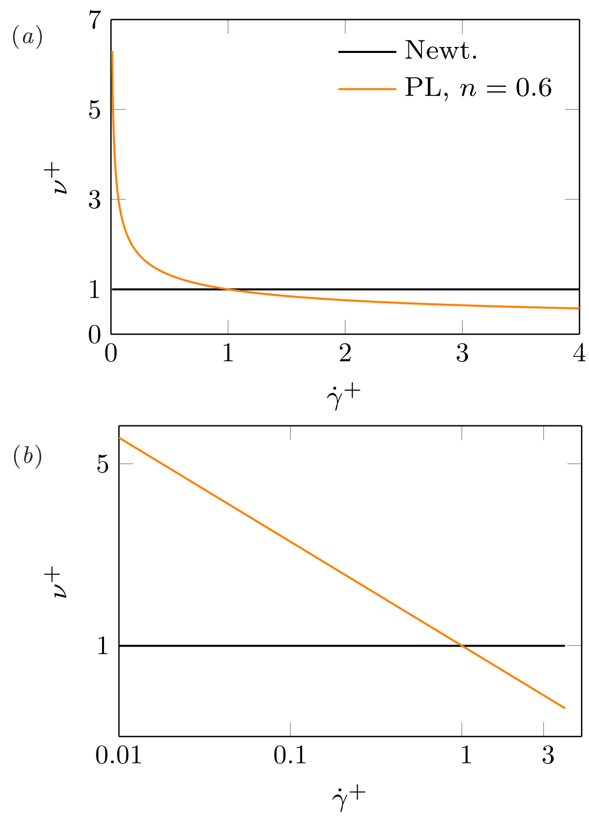

FIG. 2. Viscosity rheograms plotted for Newtonian and PL fluids on (a) linear-linear and (b) log-log axes.

C. Details of mesh, domain and time averaging

A mesh and domain independence study carried out for $Re_\tau = 323$ in Singh, Rudman, and Blackburn[8] showed that a mesh which is well-resolved for Newtonian fluid is typically adequate for shear-thinning fluids at similar Re_τ. However, a slightly longer domain is required for shear-thinning fluids compared to Newtonian ones. A domain length of $L_z \approx 12D$ is chosen here for $Re_\tau = 323$ which is supported by a domain-independence study[8] and is slightly reduced to $L_z \approx 10D$ for higher Re_τ. This corresponds to a pipe length of approx. 7700 wall units at $Re_\tau = 323$ and 15000 wall units at $Re_\tau = 750$. These values are similar to those suggested as satisfactory domain

Re_τ	Δy^+	$\Delta r\theta^+$	Δz^+	$\Delta t/(\nu_w/u^{*2})$
323	0.8–4.0	5-6	21	0.035
500	0.8–4.0	5-6	12	0.023
750	0.8–4.0	5-6	12	0.021

TABLE II. Mesh spacing and time step size in wall units used in pipe flow simulations at different Re_τ

lengths for Newtonian fluids[18]. The adequacy of the domain lengths considered is also checked via the two-point correlation of the axial velocity fluctuations:

$$\rho_{u'_z u'_z}(\Delta z) = \langle u'_z(r,\theta,z,t)u'_z(r,\theta,z+\Delta z,t)\rangle / \langle u'_z(r,\theta,z)^2\rangle. \tag{10}$$

As seen in Fig. 3, $\rho_{u'_z u'_z}$ decays to zero in each fluid for all Re_τ considered, which is evidence of adequacy of domain lengths in the current simulations.

The mesh-resolutions and time-step are given in Table II for different Re_τ. We used a mesh-resolution and time-step suggested by our assessment at $Re_\tau = 323$[19] and followed typical Newtonian values[18,20,21] at higher Re_τ. The mesh at $Re_\tau = 323$ had 300 spectral elements of 11$^{\text{th}}$-order tensor-product shape functions ($N_p = 11$) and 384 axial data planes ($N_z = 384$). The number of spectral elements were increased to 1188 for higher Re_τ and (N_p, N_z) were increased from $(9, 864)$ at $Re_\tau = 500$ to $(11, 1296)$ at $Re_\tau = 750$. The sum of the turbulent kinetic energy budget terms (see Eq. 16) is almost zero in all simulations (not shown here), which suggest the adequacy of current mesh-resolutions. The cross-sectional view of the meshes is shown in Fig. 1.

Simulations were run until the calculated instantaneous wall shear stress and bulk velocity reached a statistically steady state value before collecting averages. The time-averaged statistics were then collected for approximately 12 to 15 transit times of the domain.

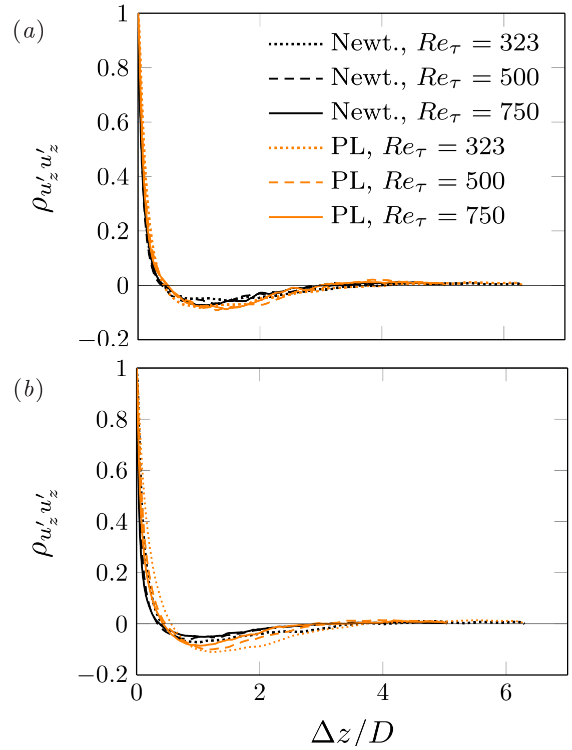

FIG. 3. Two point correlation coefficient of axial velocity fluctuations plotted as a function of separation distance $\Delta z/D$ at (a) $r/D = 0.35$ and (b) $r/D = 0.48$.

D. Comparison with the published data

For validating the numerical method, the current DNS results of Newtonian fluids are compared with those available in the literature in Figs. 4 and 5. Note that our previous study[8] compared DNS results at $Re_\tau = 323$ only with the experimental results of den Toonder and Nieuwstadt[22]; in the present study, DNS results of Newtonian fluids available in the literature at similar Reynolds number[20,23] are also included in the comparison. The current DNS results at $Re_\tau = 323$ agree well with the experimental results of den Toonder and Nieuwstadt[22] at $Re_\tau = 314$ except very close to the wall where some of the experimental results are acknowledged to be unreliable. There is a good agreement between the current results and the DNS results of Chin[23] at $Re_\tau = 500$. The current results of mean axial velocity and the turbulent kinetic energy budgets (see Section V A for the equation and the definition of different terms) are in a good agreement with El Khoury *et al.*[20]. A small deviation seen for velocity fluctuations and Reynolds stress is due to slightly higher values of Re_τ in El Khoury *et al.* compared to the current values (360 vs 323 and 550 vs 500).

III. RESULTS AND DISCUSSION

A. Instantaneous flow

The effect of Reynolds number on the instantaneous flow structures are shown in Fig. 6 for Newtonian fluid and in Fig. 7 for the shear-thinning fluid using contours of instantaneous axial velocity u_z^+ plotted in inner coordinates on an wrapped cylindrical surface at $y^+ = 10$ and in outer coordinates at a cross-section. Turbulence structures become wider and slightly longer with increasing Re_τ for each fluid. However, in outer scaling, the near-wall structures are finer for higher Re_τ as expected. With shear thinning, the near-wall turbulence structures become longer and wider, which highlights the presence of larger eddies and a narrower range of turbulent eddy sizes in shear-thinning fluid compared to Newtonian fluid. Unlike Newtonian fluids, wider and coarser turbulent structures in shear-thinning fluid are associated with higher

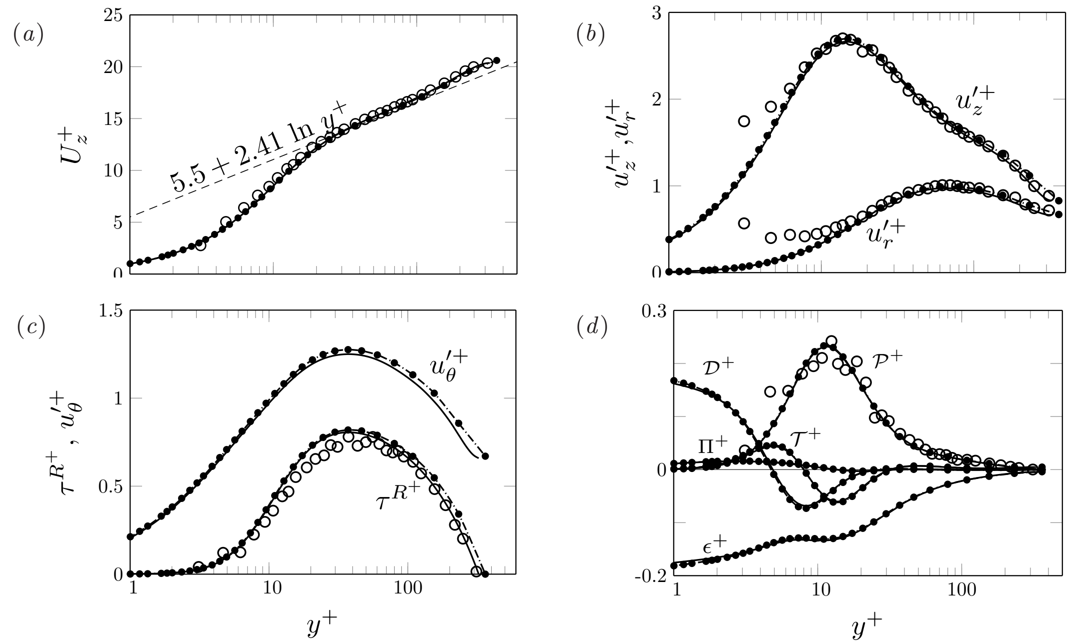

FIG. 4. Inner-scaled statistical profiles from DNS of Newtonian fluid at $Re_\tau = 323$ (solid lines), compared to experimental results of den Toonder and Nieuwstadt [22] (circles: $Re_\tau = 314$) and DNS results of El Khoury *et al.* [20] (filled circles: $Re_\tau = 360$). (a) mean axial velocity; (b) rms of axial and radial velocity fluctuations; (c) Reynolds shear stress and azimuthal velocity fluctuations (d) turbulent kinetic energy budget.

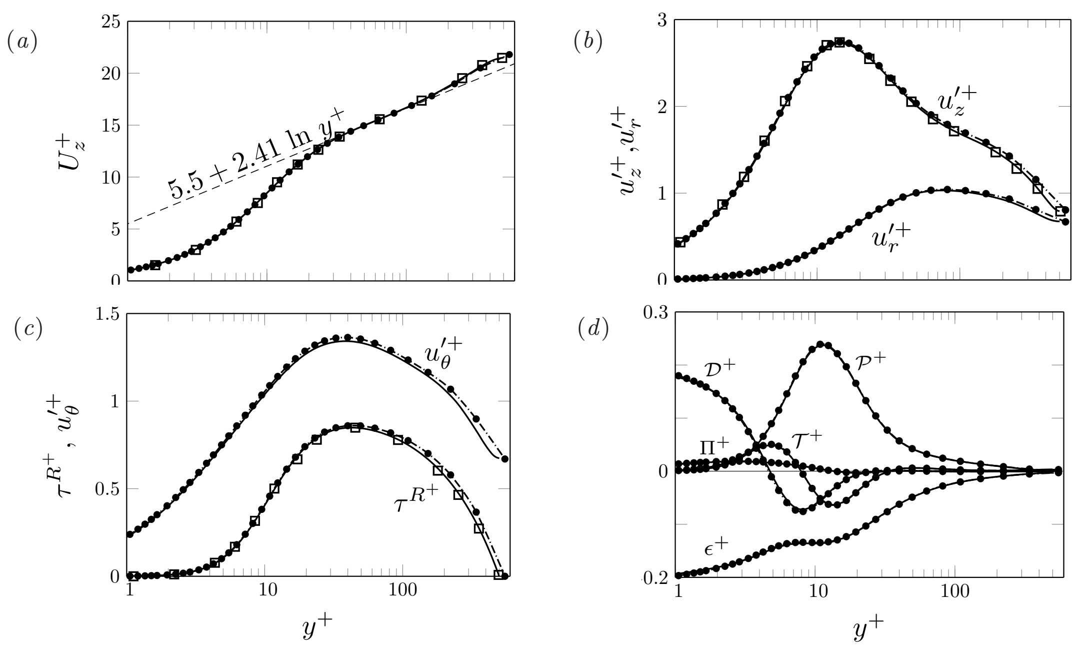

FIG. 5. Inner-scaled statistical profiles from DNS of Newtonian fluid at $Re_\tau = 500$ (solid line), compared to DNS results of El Khoury *et al.* [20] (filled circles: $Re_\tau = 550$) and Chin [23] (squares: $Re_\tau = 500$). (a) mean axial velocity; (b) rms of axial and radial velocity fluctuations; (c) Reynolds shear stress and azimuthal velocity fluctuations (d) turbulent kinetic energy budget.

turbulent kinetic energy which is a result of increased axial fluctuations[8].

The velocity integral length scale is a measure of the characteristic correlation distance between the velocity fluctuations in the flow field and can be used to quantify the information in Fig. 6 and Fig. 7. Here the streamwise integral velocity scale l_z^+ and the azimuthal integral velocity scale $l_{r\theta}^+$ are calculated by integrating the corresponding two-point correlations functions as:

$$
\begin{aligned}
l_z^+(y^+) &= \int \langle u_z'(y^+,\theta,z^+,t)u_z'(y^+,\theta,z^++\Delta z^+,t)\rangle / \langle u_z'(y^+,\theta,z^+)^2\rangle d(\Delta z^+) \\
l_{r\theta}^+(y^+) &= \int \langle u_z'(y^+,\theta,z^+,t)u_z'(y^+,\theta+\Delta\theta,z^+,t)\rangle / \langle u_z'(y^+,\theta,z^+)^2\rangle d(\Delta z^+)
\end{aligned}
\tag{11}
$$

where $\langle\rangle$ represents the spatial averaging in the azimuthal direction for l_z^+ and in the streamwise direction for $l_{r\theta}^+$. The integration is done to the point where the integrand functions first cross zero. l_z^+ and $l_{r\theta}^+$ are time-averaged for approximately $30-50$ time snapshots collected over a period of $30-50$ time units. Both the streamwise and azimuthal integral length scales l_z^+ and $l_{r\theta}^+$ increase with increasing Re_τ for each fluid, which is consistent with Figs. 6 and 7. As expected, shear-thinning fluids shows larger l_z^+ and $l_{r\theta}^+$ than Newtonian fluid at all Re_τ.

B. First order turbulence statistics

Mean axial velocity and viscosity

Inner-scaled profiles of mean axial velocity (U_z^+) and its gradient $\partial U_z^+/\partial y^+$ are presented in Fig. 9. For Newtonian fluids, it is common to subdivide the flow region into viscous sublayer ($y^+ < 5$), buffer layer ($5 < y^+ < 30$), log-layer ($30 < y^+ < 200$) and core-region ($y^+ > 200$)[24]. Additionally, the flow is divided into inner layer ($y/R < 0.1$) and outer layer ($y^+ > 50$) and there is an overlap region ($y^+ > 50$, $y/R < 0.1$). Although this kind of delineation is not obvious for GN fluids[8], we use the same subdivision here for ease of discussion. The mean axial velocity profiles are almost independent of Re_τ in the viscous sublayer for each fluid and outside the viscous sublayer, the U_z^+ profiles deviate below with increasing Re_τ. The mean axial velocity U_z^+ is larger for the PL fluid which leads to a larger bulk velocity U_b^+ compared to Newtonian fluid (Table I). The effect of Re_τ on U_z^+ profiles diminishes at larger Re_τ and it seems unlikely that the inner-scaled U_z^+ profiles of two fluids will ever collapse with increasing Re_τ. The U_z^+ profiles of each fluid are expected to become Re_τ-independent with further increasing Re_τ, which suggests the possibility of defining a new non-dimensionalisation to collapse the non-Newtonian and Newtonian profiles, however, we are not aware of any such theoretical analysis for GN fluids.

An examination of mean axial velocity profiles via their gradients shows that the slope of the mean axial velocity is also independent of the Reynolds number for both fluids (Fig. 9 *b*). Shear thinning increases the mean axial velocity gradient above unity in the viscous sublayer, which is a result of non-zero turbulent viscous stress there as explained in Singh, Rudman, and Blackburn [8].

From Fig. 9, the mean axial velocity appears to approximately follow a log-law profile $A \ln y^+ + B$ in the overlap layer for both fluids with similar slope A. This is further investigated via the log-law indicator function, $\Xi = y^+\partial U_z^+/\partial y^+$, that is constant in where the U_z^+ profiles follow a log-law (log region). Fig. 10 (a) shows that for both fluids, the mean axial velocity profiles follow a log-law scaling only in a narrow range of y^+ which widens with increasing Re_τ. This is consistent with the findings of Chin, Monty, and Ooi [21], Ahn *et al.* [25] and Zagarola, Perry, and Smits [26] for Newtonian fluids. The plateau in the Ξ profile is usually taken as the slope parameter A in the log-law[21]. As seen in Fig. 10 (a), the slope parameter, A, slightly decreases with increasing Re_τ for both the fluids and slightly increases with shear thinning ($A = 2.52$ for PL fluid vs. 2.41 for Newtonian fluid at $Re_\tau = 750$). The location where the plateau in Ξ is reached shifts away from the wall with shear thinning.

Although a log-law scaling is commonly assumed, at the present Reynolds numbers, a log-law correlation is not convincing. Therefore, we have alternately considered a power-law scaling $U_z^+ = C{y^+}^\Gamma$ where C and Γ are constants. It is worth noting that theoretically a power-law scaling is obtained in general and a log-law scaling is obtained asymptotically for an infinite Reynolds number[27]. However, the existence of both the scalings has been suggested, but in different ranges of y^+[28]. The validity of a power-law scaling for the current results is checked via its indicator function $\Gamma = (y^+/U_z^+)\partial U_z^+/\partial y^+$ plotted in Fig. 10 (b). The figure shows that the mean axial velocity profiles approximately follow a power-law scaling over a somewhat wider range of y^+ than a log-law scaling. Therefore, a power-law correlation is perhaps slightly better than a log-law at the Reynolds number considered here. The power-law coefficient Γ is almost independent of Re_τ and slightly decreases with shear thinning ($\Gamma = 0.15$ for Newtonian vs. 0.14 for PL fluid).

In turbulent boundary layer flows of Newtonian fluids, the velocity defect $U_{z,CL} - U_z$ where $U_{z,CL}$ is the mean centre line velocity, become independent of the viscosity in the outer layer[24], which is also seen here in Fig. 11. Velocity defect profiles of Newtonian and PL fluids collapse in this region, which suggests that the velocity defect in

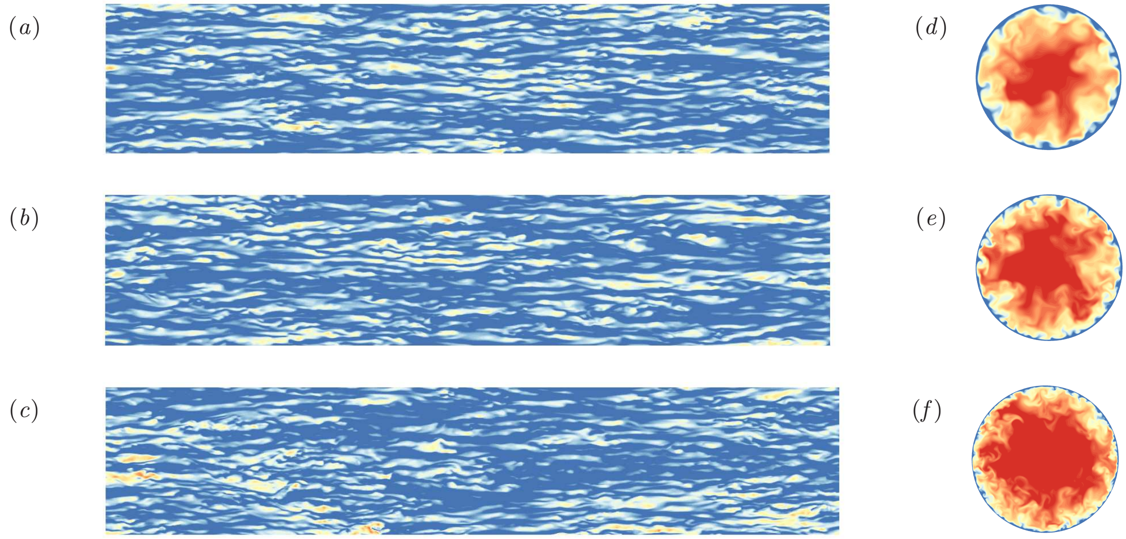

FIG. 6. Contours of inner-scaled instantaneous axial velocity u_z^+ plotted (a–c) in inner coordinates on a developed cylindrical surface $z^+ - r\theta^+$ at $y^+ = 10$ and (d–f) in outer coordinates on a cross-section for a Newtonian fluid at (from top to bottom) $Re_\tau = 323, 500$ and 750. For a–c, the flow is from left to right and the region is 7000 wall units long and 1600 wall units wide. The contours levels vary from blue to red with the values 8 to 20.

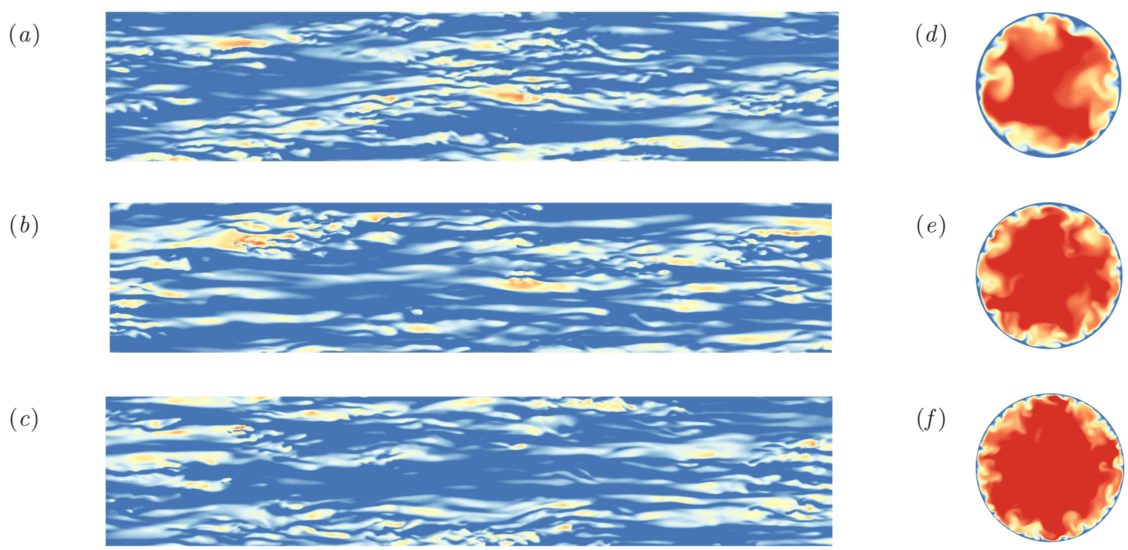

FIG. 7. Contours of inner-scaled instantaneous axial velocity u_z^+ plotted (a–c) in inner coordinates on a developed cylindrical surface $z^+ - r\theta^+$ at $y^+ = 10$ and (d–f) in outer coordinates on a cross-section for PL fluid at (from top to bottom) $Re_\tau = 323, 500$ and 750. For a–c, the flow is from left to right and the region is 7000 wall units long and 1600 wall units wide. The contours levels vary from blue to red with the values 8 to 20.

the outer layer is largely independent of the fluid rheology despite the PL fluid showing very large viscosity (as will be discussed in the following). This lends support to the idea that the larger inner-scaled mean axial velocity and the bulk velocity shown by PL fluid as compared to Newtonian fluid (see Table. I and Fig. 9 a) are largely due to the differences in the flows of the two fluids near the wall.

Overall the mean axial velocity profiles of both Newtonian and shear-thinning fluids show a similar Re_τ-dependence, however for each Re_τ, the differences between the profiles of two fluids are clearly evident. Shear-thinning fluid exhibit larger mean axial velocity U_z^+ in outer flow region than Newtonian fluid.

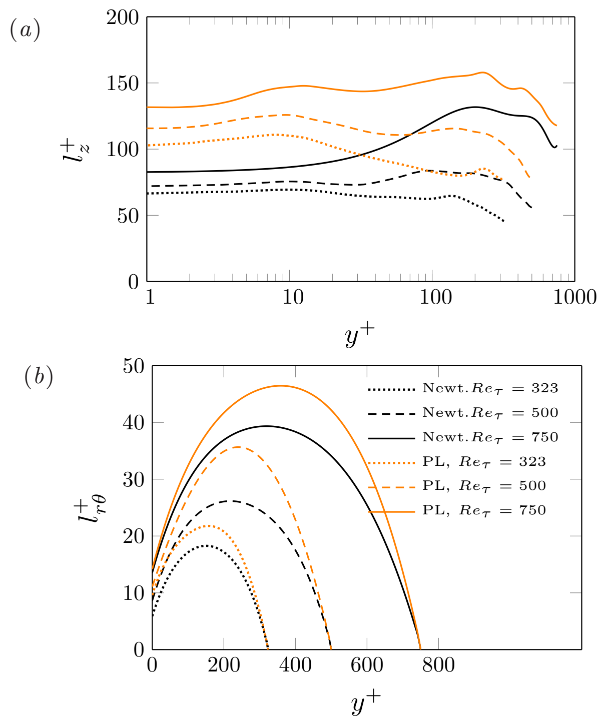

FIG. 8. (a) Streamwise and (b) azimuthal integral length scales of axial velocity fluctuations plotted as a function of y^+.

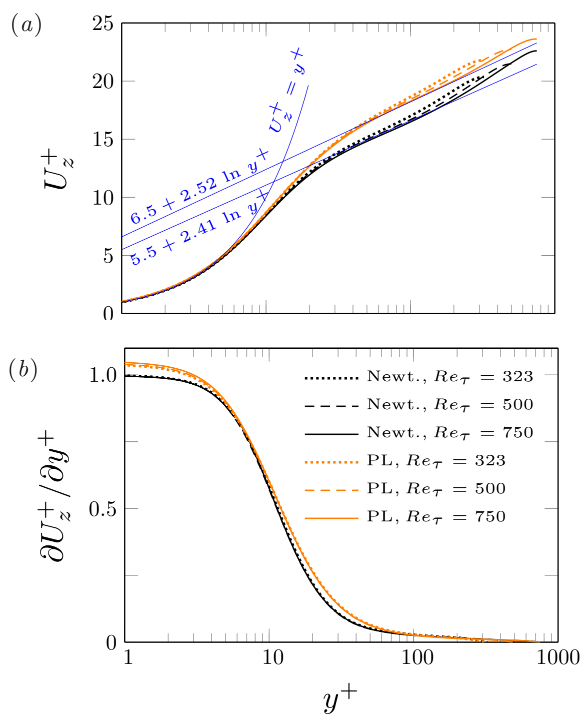

FIG. 9. Profiles of the inner-scaled (a) mean axial velocity and (b) mean axial velocity gradient plotted for Newtonian (black lines) and PL fluids (orange lines). Blue lines in (a) show the law of wall with the slope parameter determined in Fig. 10 (a) for $Re_\tau = 750$.

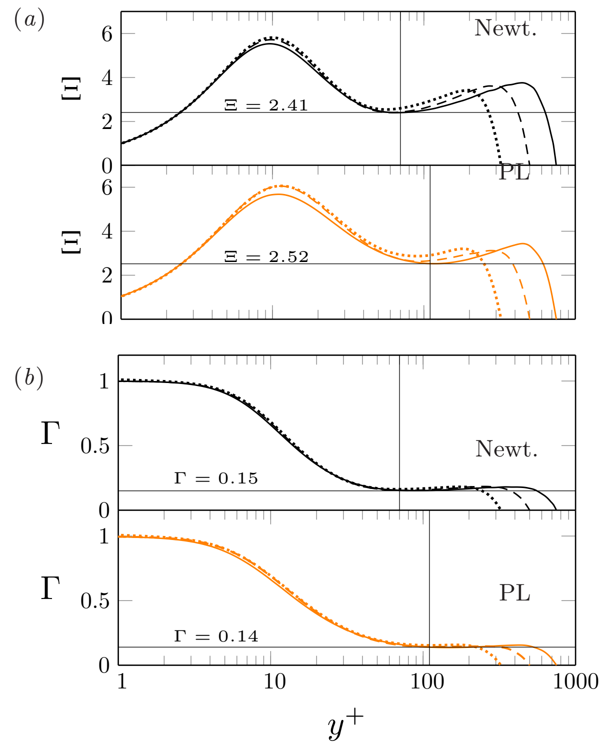

FIG. 10. (a) log-law and (b) power-law indicator functions for Newtonian and PL fluids. Vertical lines show the location where the labelled values are read.

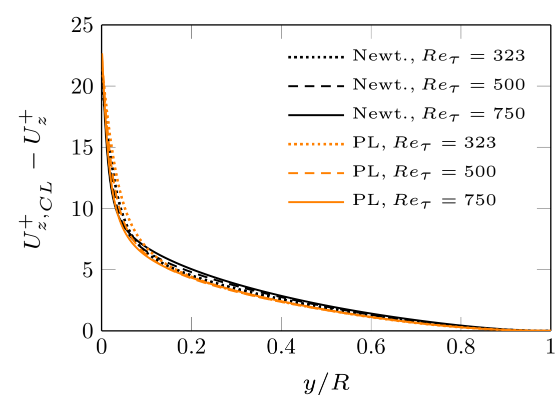

FIG. 11. Profiles of the velocity defect plotted in outer coordinates for Newtonian and PL fluids at different Re_τ.

Similar to the mean axial velocity, the mean viscosity profile of shear-thinning fluid is also almost independent of Re_τ in the viscous sublayer and is slightly higher than the Newtonian viscosity ($\nu^+ = 1$) (Fig. 12). The mean viscosity profiles show a log-like region in buffer and log layers and the extent of this log-like region increases with increasing Re_τ. The mean viscosity profiles collapse for different Re_τ below the wake region. The reason for the functional form of the collapsed mean viscosity profiles is not obvious.

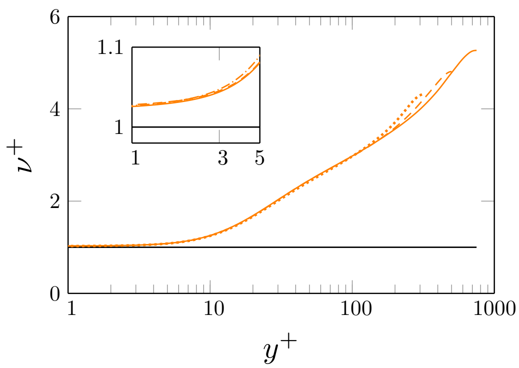

FIG. 12. Profiles of the normalised mean viscosity plotted for PL fluid at different Re_τ. For line legend see Fig. 9.

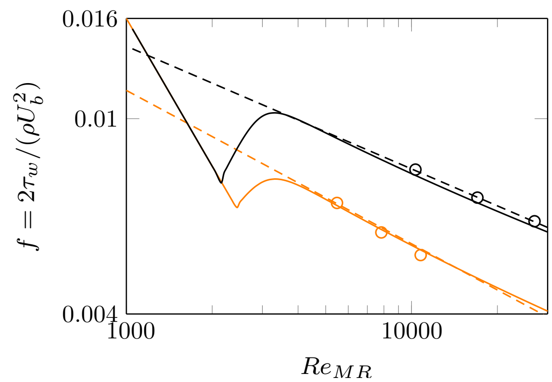

FIG. 13. Comparison of the friction factor obtained via DNS (circles) and those of the Dodge & Metzner correlation (solid lines) and the Anbarlooei & Cruz correlation (dashed lines) for Newtonian (black lines) and PL fluids (orange lines).

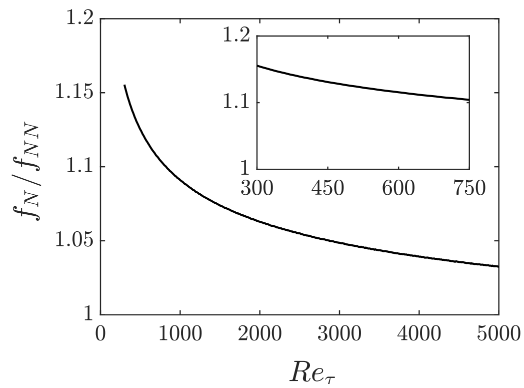

FIG. 14. Ratio of friction factors for Newtonian and PL fluids obtained from the correlation (Eq. 13) plotted against Re_τ with the inset figure showing a closer look in the Re_τ-range considered in this study.

Friction factor

Using the non-dimensionalisation based on wall units, friction factor can be written as $f = 2/{U_b^+}^2$ where U_b^+ is the area weighted averaged of the mean axial velocity U_z^+. The DNS predictions of the friction factor are shown in Fig. 13. With increasing Re_τ, U_z^+ integrates to larger y^+ (Fig. 9 *a*) which gives a higher U_b^+ and hence a lower friction factor f for higher Re_τ. Due to the increase in U_z^+ with shear thinning in the log-layer and core-region, U_b^+ is larger and the friction factor is lower for the PL fluid compared to Newtonian fluid.

Several empirical correlations have been proposed for PL fluids[29] in which the Dodge & Metzner correlation[5] (Eq. 4) has been found to agree well with the experiments[6]. For Newtonian fluids, the Dodge & Metzner correlation reduces to the Nikuradse correlation. Although the Dodge & Metzner correlation is widely used for PL fluids, it does not have a theoretical support[30]. Anbarlooei & Cruz[30] proposed the following alternate friction factor correlation based on the Newtonian Blasius correlation.

$$f = \left(0.102 - 0.033n + \frac{0.01}{n}\right) \Big/ Re_{MR}^{1/2(n+1)} \tag{12}$$

DNS predictions of friction factor are compared with these correlations in Fig. 13. The current predictions for Newtonian fluids agree better with the Blasius correlation than Nikuradse's correlation, which is consistent with the findings of El Khoury *et al.*[20] for the Reynolds numbers considered here. Both Dodge & Metzner and Anbarlooei & Cruz correlations agree well with each other for the shear-thinning fluid in $Re_{MR} \lesssim 100\,000$. The agreement between DNS and the correlations is good at $Re_\tau = 323$, however for higher Re_τ, DNS slightly under-predicts the friction factor compared to the correlations.

The ratio of DNS predictions of the friction factor for Newtonian and PL fluids was observed to be only slightly decreasing with increasing Re_τ in Table I. This is further analysed using the Dodge & Metzner correlation which can be expressed as an explicit function of Re_τ as:

$$\frac{1}{\sqrt{f}} = \frac{4}{n^{0.75}} \log_{10}\left[\frac{Re_\tau^n 2^{4-n/2}}{(3+1/n)^n}\right] - \frac{0.4}{n^{1.2}}. \tag{13}$$

The ratio of f for Newtonian and PL fluids is plotted against Re_τ in Fig. 14 which shows that in the range of Re_τ considered here, the ratio f_N/f_{NN} decreases very slowly (see the inset figure). The decrease in f_N/f_{NN} with Re_τ becomes slower as Re_τ is increased and it appears that f_N/f_{NN} will approach to unity only for an infinite Re_τ.

Mean shear stress budget

As explained in Singh, Rudman, and Blackburn[8], the Reynolds decomposition for velocity $\boldsymbol{v} = \boldsymbol{V} + \boldsymbol{v'}$; viscosity $\nu = \bar{\nu} + \nu'$ and the rate of strain tensor $\boldsymbol{s} = \boldsymbol{S} + \boldsymbol{s'}$, where defining $\boldsymbol{V}$, $\bar{\nu}$ and $\boldsymbol{S}$ as the time-averaged quantities, leads to the following expression for the (r,z) component of the mean shear stress:

$$\tau_{rz}^{+} = \tau_{rz}^{v^+} + \tau_{rz}^{R^+} + \tau_{rz}^{fv^+} = \frac{r}{R} = \left(1 - \frac{y^+}{R^+}\right). \qquad (14)$$

where $\tau_{rz}^{v^+} = \bar{\nu}^+ \partial U_z^+/\partial y^+$, $\tau_{rz}^{R^+} = -v_r^+ v_z^+$ and $\tau_{rz}^{fv^+} = 2\overline{\nu' s'_{rz}}^+$. Since except (r,z), all other components of the mean shear stress are zero in a pipe flow, the subscript rz is dropped in the following discussion for clarity. Note that τ_{rz}^{+} is independent of the fluid rheology and the profiles of τ_{rz}^{+} of both Newtonian and shear-thinning fluids will collapse on top of each other for a fixed Re_τ as shown and discussed in Singh, Rudman, and Blackburn[8] for $Re_\tau = 323$.

The profiles of the inner-scaled mean shear stress components in the (r,z) direction are plotted in Fig. 15 for both fluids at different Re_τ. As expected from the results of the mean axial velocity gradient and the mean viscosity (Fig. 9 *b* and Fig. 12), the mean viscous stress τ^{v^+} is almost independent of Reynolds number for both fluids except in the viscous sublayer. In the viscous sublayer, τ^{v^+} slightly increases with increasing Re_τ for PL fluid, which is due to an increase in the magnitude of the turbulent viscous stress τ^{fv^+} (Fig. 15 *c*).

Compared to τ^{v^+} and τ^{fv^+}, profiles of the Reynolds shear stress, τ^{R^+}, show a large Re_τ-dependence. For each fluid, τ^{R^+} increases significantly in the log layer and core region and the peak moves further away from the wall with increasing Re_τ. This trend is consistent with past studies of Newtonian fluids[20,21]. Differences between the τ^{R^+} profiles of two fluids disappear in the outer log-layer and core region for all Re_τ supporting the idea that the effect of shear-thinning is confined near the wall. The y^+ location where τ^{R^+} profiles of two fluids start overlapping each other is almost independent of Re_τ, which suggests that the region where the PL rheology have a major influence on the flow is independent of the Reynolds number, however, this needs to be confirmed. Overall, the Re_τ dependence of the mean shear stresses is similar for both fluids.

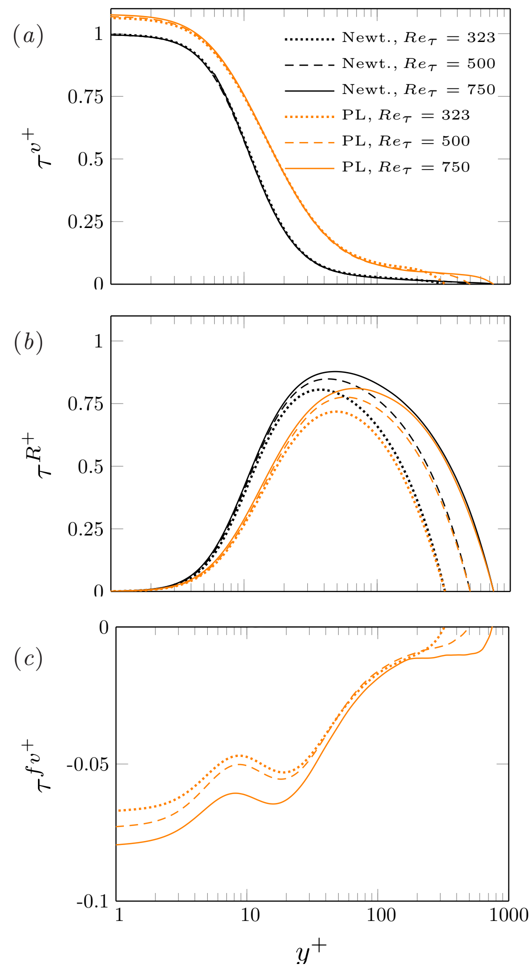

FIG. 15. Profiles of the (*a*) mean viscous stress τ^{v^+} (*b*) Reynolds shear stress τ^{R^+} and (*c*) turbulent viscous stress τ^{fv^+} plotted for Newtonian and PL fluids at different Re_τ.

Turbulence intensities and viscosity fluctuations

Turbulence intensity profiles of both fluids are also similarly affected with increasing Re_τ with each component increasing with Re_τ (Fig. 16). Similar to τ^{R^+}, the axial turbulence intensity $u_z'^+$ shows a large Re_τ-dependence only for $y^+ \gtrsim 30$. The location of maximum $u_z'^+$ is independent of Re_τ for each fluid. The effect of shear-thinning on $u_z'^+$ disappears near the pipe centre for $y^+ \gtrsim 200$. The same is seen via the axial turbulence intensity profiles plotted against y/R, which almost collapse in the outer layer for Newtonian and PL fluids and for different Re_τ (Fig. 16 *b*).

Unlike $u_z'^+$, profiles of the radial and azimuthal turbulence intensities, $u_r'^+$ and $u_\theta'^+$, do not collapse near the pipe centre for the two fluids, however, however, the gap between the profiles of two fluids becomes smaller at higher Re_τ. The radial and azimuthal turbulence intensity profiles may collapse for Newtonian and PL fluids in the outer layer but at Reynolds numbers larger than considered here (Fig. 16 b,d,e). Profiles of the root mean square viscosity fluctuations are marginally affected with increasing Re_τ (Fig. 17 *a*) with the differences seen more clearly when normalised by the local mean viscosity $\bar{\nu}^+$ (Fig. 17 *b*).

Overall these results show clear differences between the flow of shear-thinning and Newtonian fluids at all Re_τ considered here. The effect of shear thinning on turbulence intensity profiles diminishes with increasing Re_τ especially in the log-layer and core region, however, it is still significant at the highest Re_τ considered here ($Re_\tau = 750$).

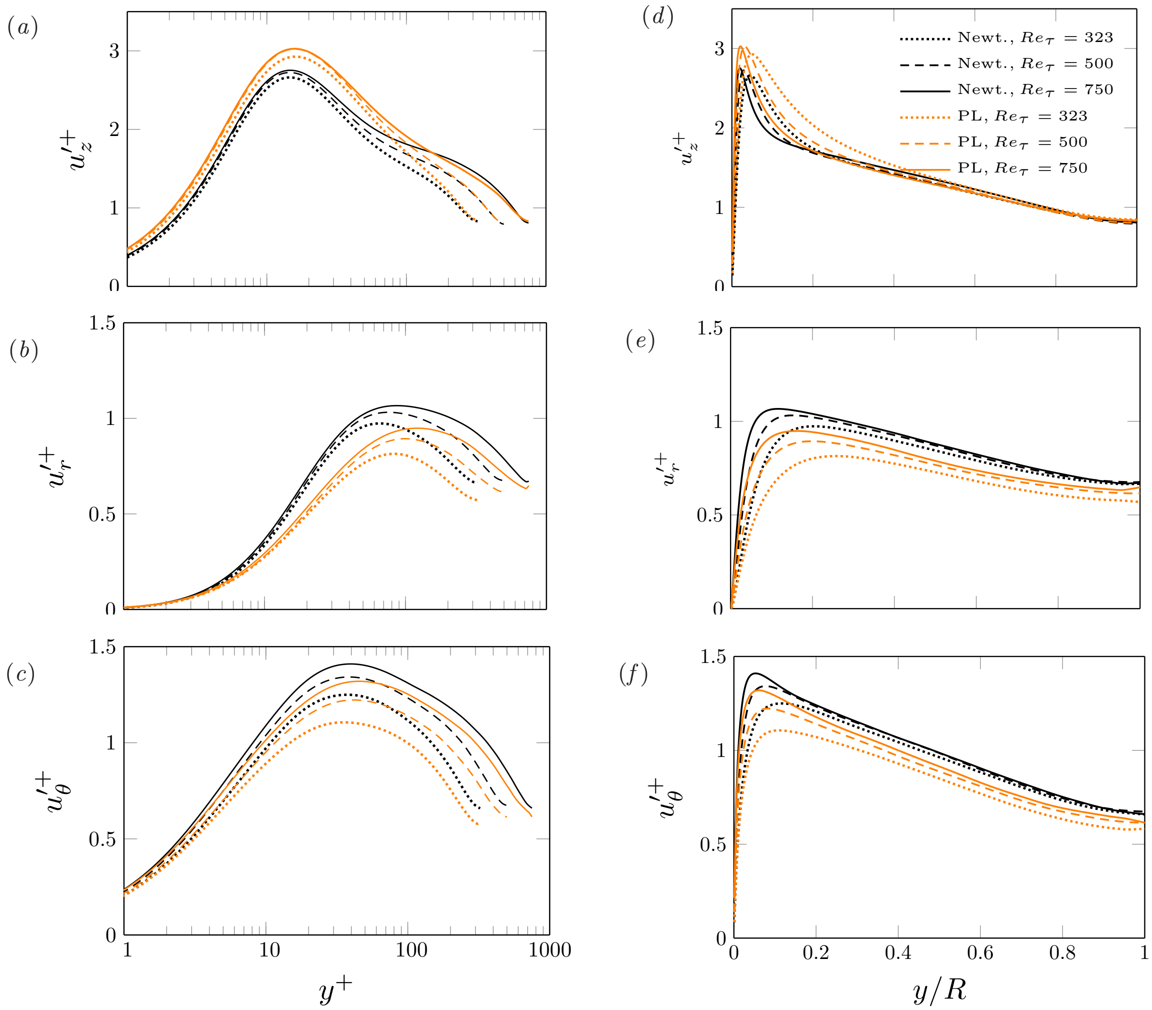

FIG. 16. Profiles of turbulence intensities plotted as a function of (a)–(c) y^+ and (d)–(f) y/R for Newtonian and PL fluids at different Re_τ.

C. Higher order turbulence statistics

A detailed discussion on the mean flow kinetic energy (MFKE) and the turbulent kinetic energy (TKE) budgets is available for PL fluids in Singh, Rudman, and Blackburn [8] at a fixed Reynolds number. Here, we analyse the effect of Reynolds number on these energy budgets but to keep the paper short, the results are included as an appendix in Sec. V where the main points are as follows.

Similar to the results of the first order turbulence statistics presented above, profiles of the different terms in the mean flow kinetic energy (MFKE) and the turbulent kinetic energy (TKE) budget terms show a similar Re_τ-dependence for Newtonian and PL fluids. In the MFKE budget, only the MFKE production and its transport via the Reynolds stress (turbulent transport of MFKE) show a large Re_τ-independence. The MFKE production by definition $(U_z^+\partial P^+/\partial z^+)$ follows the same trend as the mean axial velocity U_z^+. Similar to the Reynolds shear stress, the turbulent transport of MFKE $(\mathcal{T}^m = -\partial(U_i\overline{u_i'u_j'})/\partial x_j)$ show a large Re_τ-dependence only for $y^+ \gtrsim 30$ and the shear-thinning effect disappears in the outer layer and core region. The non-Newtonian terms (terms introduced due to viscosity fluctuations) remain small compared to other terms at all Re_τ and thus, only marginally contribute in the MFKE budget.

The turbulent kinetic energy budgets show Reynolds number and shear-thinning dependence only near the wall. The Reynolds number effect disappears for $y^+ \lesssim 30$ whereas the shear-thinning effect can be seen until $y^+ \approx 100$. The contribution of the non-Newtonian terms (terms introduced due to viscosity fluctuations) remains small compared to turbulent production and dissipation, however, they increase in magnitude with increasing Re_τ. Over the results show that the shear-thinning effect on the energy budgets is unlikely to disappear even at very high Reynolds number.

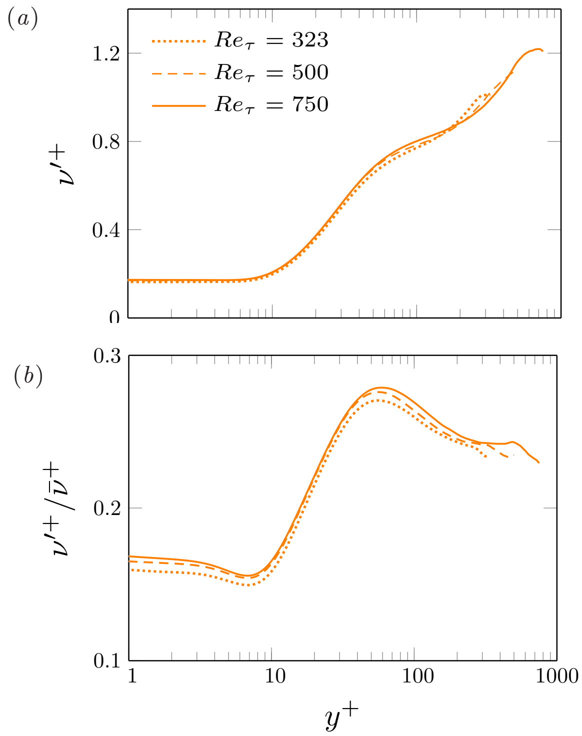

FIG. 17. Profiles of the rms viscosity fluctuations normalised by (a) the nominal wall viscosity and (b) the local mean viscosity plotted for PL fluid at different Re_τ.

IV. SUMMARY AND CONCLUSIONS

Due to the difficulties in optical measurements in GN fluids, most experimental studies of turbulent pipe flow of GN fluids were limited to measuring turbulent friction factor and much insight has been gained via direct numerical simulations. Past DNS studies of GN fluids showed distinguishably different flow behaviour for GN fluids compared to Newtonian ones. The most notable differences were that the mean axial velocity profiles shift above the Newtonian profiles in the log-layer, axial turbulence intensity increase but the radial and the azimuthal components decrease with shear-thinning. The GN rheology was found to affect the turbulent kinetic energy budget mostly in the near wall-region. Despite of the significant advancement of computational technology, much of the DNS data available for GN fluids is limited to low Reynolds numbers ($Re_G < 12\,000$). As the Reynolds number increases, the viscous region becomes smaller in outer units compared to the pipe radius, it is not clear whether the observed shear-thinning effects will persist at higher Reynolds number. This is the fundamental question we attempt to answer in this study. Simulations carried out for Newtonian and shear-thinning PL ($n = 0.6$) fluids for $Re_\tau = 323, 500$ and 750 provide strong evidence that the effect of shear-thinning will not disappear with increasing Reynolds number. There is a persistent difference between the two sets of curves in the near-wall region that stems from a difference in rheologies, and which is mostly independent of Reynolds number. It seems unlikely that the inner-scaled mean axial velocity profiles will ever collapse to a common curve for Newtonian and PL fluids. This phenomenon is consistent with the predictions of the Dodge & Metzner correlation. For the Reynolds number range considered here, the mean axial velocity profiles are found in a better agreement with a power-law scaling ($U_z^+ = Cy^{+\Gamma}$) than a log-law scaling ($A \ln y^+ + B$) for each fluid. With increasing Reynolds number, the mean axial velocity tend to become independent of the Reynolds number, which suggests the possibility of defining a new non-dimensionalisation to collapse the Newtonian and non-Newtonian mean axial velocity profiles at larger Re_τ. However, data for a range of flow indices n and larger Re_τ are required to propose such non-dimensionalisation and therefore, it remains future work.

In the mean shear stresses, the Reynolds shear stress is the most affected by varying Reynolds number and it becomes independent of the shear-thinning rheology by $y^+ \approx 200$ irrespective of the Reynolds number. Profiles of the axial turbulence intensity when plotted in outer units collapse in the outer layer for Newtonian and PL fluids at all Reynolds number. The radial and the azimuthal turbulence intensity profiles are also expected to follow a similar trend but at larger Reynolds numbers than considered here. The y^+ location up to which varying Reynolds number has the most prominent effect on the turbulent kinetic energy budget is larger for the shear-thinning fluid compared to Newtonian fluid ($y^+ \approx 30$ vs $y^+ \approx 20$). However, for a given Reynolds number, the shear-thinning effects on the turbulent kinetic energy budget persist until $y^+ \approx 200$ and the Newtonian and PL profiles collapse on top of each other beyond this y^+. Interestingly, in this y^+ range ($y^+ \lesssim 200$), the mean viscosity profiles are largely independent of the Reynolds number. The reason for the functional form of the collapsed mean viscosity profiles is not obvious. However, the Reynolds number independence of the mean viscosity profiles and small contribution of the viscosity fluctuations in the mean shear stress and the energy budgets have implications on RANS and LES of GN fluids. These results suggest that the effect of shear-thinning rheology in RANS or LES can be captured via an appropriate mean viscosity model in the inner region, and such mean viscosity model for a fluid can be independent of the Reynolds number.

ACKNOWLEDGMENTS

Computations were carried out using the resources provided by the Pawsey Supercomputing Centre with funding from the Australian Government and the Government of Western Australia via the NCI merit allocation scheme grant number D77. We gratefully acknowledge

the resources and their support.

[1] R. Chhabra and J. Richardson, *Non-Newtonian Flow and Applied Rheology (Second Edition)* (Elsevier, 2008).
[2] J. Singh, M. Rudman, H. M. Blackburn, A. Chryss, L. Pullum, and L. J. W. Graham, "The importance of rheology characterization in predicting turbulent pipe flow of generalized Newtonian fluids," J. Non-Newt. Fluid Mech. **232**, 11–21 (2016).
[3] A. B. Metzner and J. C. Reed, "Flow of non-Newtonian fluids – correlations for laminar, transition and turbulent flow regimes," A. I. Ch. E. J. **1**, 434–444 (1955).
[4] N. El-Emam, A. Kamel, A. El-Shafei, and A. El-Batrawy, "New equation calculates friction factor for turbulent flow on non-Newtonian fluids," Oil and Gas J. **101**, 74 (2003).
[5] D. W. Dodge and A. B. Metzner, "Turbulent flow of non-Newtonian systems," A. I. Ch. E. J. **5**, 189–204 (1959).
[6] E. J. Garcia and J. F. Steffe, "Comparison of friction factor equations for non-Newtonian fluids in pipe flow," J. Food Process Eng. **9**, 93–120 (1986).
[7] D. C. Bogue and A. B. Metzner, "Velocity profiles in turbulent pipe flow. Newtonian and non-Newtonian fluids," Ind. Eng. Chem. Fundam. **2**, 143–149 (1963).
[8] J. Singh, M. Rudman, and H. Blackburn, "The influence of shear-dependent rheology on turbulent pipe flow," J. Fluid Mech. **822**, 848–879 (2017).
[9] M. Rudman, H. M. Blackburn, L. J. W. Graham, and L. Pullum, "Turbulent pipe flow of non-Newtonian fluids," J. Non-Newt. Fluid Mech. **118**, 33–48 (2004).
[10] M. Rudman and H. M. Blackburn, "Direct numerical simulation of turbulent non-Newtonian flow using a spectral element method," Appl. Math. Mod. **30**, 1229–1248 (2006).
[11] A. A. Gavrilov and V. Y. Rudyak, "Direct numerical simulation of the turbulent flows of power-law fluids in a circular pipe," Thermoph. and Aeromech. **23**, 473–486 (2016).
[12] J. T. Park, R. J. Mannheimer, T. A. Grimley, and T. B. Morrow, "Pipe flow measurements of a transparent non-Newtonian slurry," ASME J. Fluid Engng **111**, 331 (1989).
[13] F. T. Pinho and J. H. Whitelaw, "Flow of non-Newtonian fluids in a pipe," J. Non-Newt. Fluid Mech. **34**, 129–144 (1990).
[14] J. Singh, M. Rudman, and H. Blackburn, "The effect of yield stress on pipe flow turbulence for generalised Newtonian fluids," J. Non-Newt. Fluid Mech. **249**, 53–62 (2017).
[15] J. Singh, M. Rudman, and H. M. Blackburn, "The rheology dependent region in turbulent pipe flow of a generalised Newtonian fluid," in *Australasian Fluid Mech. Conf. (04 December 2016 to 7 December 2016)* (Univ. of Western Australia, Perth, 2016).
[16] R. I. Tanner and J. F. Milthorpe, "Numerical simulation of the flow of fluids with yield stress," in *Proc. 3rd Int. Conf., Seattle, Pineridge Press, Swansea* (1983) pp. 680–690.
[17] H. M. Blackburn and S. J. Sherwin, "Formulation of a Galerkin spectral element–Fourier method for three-dimensional incompressible flows in cylindrical geometries," J. Comput. Phys. **197**, 759–778 (2004).
[18] C. Chin, A. S. H. Ooi, I. Marusic, and H. M. Blackburn, "The influence of pipe length on turbulence statistics computed from direct numerical simulation data," Phys. Fluids **22** (2010).
[19] J. Singh, *Turbulent flow of Generalised Newtonian fluids through pipes and open channels*, Ph.D. thesis, Monash Univ. (2017).
[20] G. K. El Khoury, P. Schlatter, A. Noorani, P. F. Fischer, G. Brethouwer, and A. V. Johansson, "Direct numerical simulation of turbulent pipe flow at moderately high Reynolds numbers," Flow, Turb. and Comb. **91**, 475–495 (2013).
[21] C. Chin, J. Monty, and A. Ooi, "Reynolds number effects in DNS of pipe flow and comparison with channels and boundary layers," Intnl J. Heat Fluid Flow **45**, 33–40 (2014).
[22] J. M. J. den Toonder and F. T. M. Nieuwstadt, "Reynolds number effects in a turbulent pipe flow for low to moderate *Re*," Phys. Fluids **9**, 3398–3409 (1997).
[23] C. Chin, *Numerical study of internal wall-bounded turbulent flows*, Ph.D. thesis, The Univ. of Melbourne, Australia (2011).
[24] S. B. Pope, *Turbulent flows* (Cambridge University Press, 2000).
[25] J. Ahn, J. H. Lee, J. Lee, J.-h. Kang, and H. J. Sung, "Direct numerical simulation of a 30R long turbulent pipe flow at $\mathrm{Re}_\tau =$ 3008," Phys. Fluids **27**, 065110 (2015).
[26] M. Zagarola, A. Perry, and A. Smits, "Log laws or power laws: The scaling in the overlap region," Phys. Fluids **9**, 2094–2100 (1997).
[27] G. I. Barenblatt, *Scaling, Self-similarity, and Intermediate Asymptotics: Dimensional Analysis and Intermediate Asymptotics*, Vol. 14 (Cambridge University Press, 1996).
[28] M. V. Zagarola and A. J. Smits, "Mean-flow scaling of turbulent pipe flow," J. Fluid Mech. **373**, 33–79 (1998).
[29] P. Gao and J. Zhang, "New assessment of friction factor correlations for power law fluids in turbulent pipe flow: A statistical approach," J. Central South Univ. of Tech. **14**, 77–81 (2007).
[30] H. R. Anbarlooei, D. Cruz, F. Ramos, and A. P. S. Freire, "Phenomenological Blasius-type friction equation for turbulent power-law fluid flows," Phys. Rev. E **92**, 063006 (2015).
[31] F. T. Pinho, "A GNF framework for turbulent flow models of drag-reducing fluids and a proposal for a k–ε type closure," J. Non-Newt. Fluid Mech. **114**, 149–184 (2003).
[32] P. A. Davidson, *Turbulence: An Introduction for Scientists and Engineers* (Oxford University Press, 2015).
[33] J. G. M. Eggels, *Direct and Large Eddy Simulation of Turbulent Flow in a Cylindrical Pipe Geometry*, Ph.D. thesis, Delft University (1994).

V. APPENDIX.

A. Energy budgets

The equations for the mean flow and the turbulent kinetic energy budgets are described in detail in Singh, Rudman, and Blackburn[8], Pinho[31] and only a brief overview is given here to introduce terms required in the later discussion.

Using the Reynolds decomposition, the total kinetic energy per unit mass $q = u_i u_i/2$ is written as $\bar{q} = K + k$ where $K = U_i U_i/2$ is the mean flow kinetic energy (MFKE) and $k = \overline{u_i' u_i'}/2$ is the turbulent kinetic energy (TKE). For a steady axially homogeneous flow of non-Newtonian fluid, the mean flow kinetic energy budget equation is written as:

$$\overbrace{-U_j \frac{\partial P}{\partial x_j}}^{W_{dp/dz}} + \overbrace{\left(-\frac{\partial U_i \overline{u_i' u_j'}}{\partial x_j}\right)}^{\mathcal{T}^m} + \overbrace{2\frac{\partial \bar{\nu} S_{ij} U_i}{\partial x_j}}^{\mathcal{D}^m} + \overbrace{(-2\bar{\nu} S_{ij} S_{ij})}^{\epsilon^m} + \overbrace{\overline{u_i' u_j'} S_{ij}}^{-\mathcal{P}} + \overbrace{2\frac{\partial U_i \overline{\nu' s_{ij}'}}{\partial x_j}}^{\Upsilon^m_{nn}} + \overbrace{(-2\overline{\nu' s_{ij}'} S_{ij})}^{\chi_{nn}} = 0, \tag{15}$$

where a subscript nn is used for terms which are non-zero only for a non-Newtonian fluid. The following terminology is used for different terms in Eq. 15:

$W^+_{dp/dz}$**:** the mean flow energy production;

$\mathcal{T}^m$**:** turbulent transport;

$\mathcal{D}^m$**:** the mean viscous transport;

ϵ^m**:** the mean viscous dissipation;

$-\mathcal{P}$**:** turbulent energy transfer or negative of turbulent kinetic energy production.

Υ^m_{nn}**:** the turbulent viscous stress transport;

χ_{nn}**:** The mean shear turbulent viscous dissipation;

Similarly, the turbulent kinetic energy budget equation for a steady axially homogeneous flow of a non-Newtonian fluid can be shown to be[8]:

$$\overbrace{-\overline{u_i'u_j'}S_{ij}}^{\mathcal{P}}+\Bigg\{\overbrace{-\frac{1}{2}\frac{\partial\overline{u_i'u_i'u_j'}}{\partial x_j}}^{\mathcal{T}}\overbrace{-\frac{\partial\overline{p'u_j'}}{\partial x_j}}^{\Pi}\overbrace{+\frac{\partial(2\bar{\nu}\overline{s_{ij}'u_i'})}{\partial x_j}}^{\mathcal{D}}\Bigg\}\overbrace{-2\bar{\nu}\overline{s_{ij}'s_{ij}'}}^{\epsilon}$$
$$+\Bigg\{\overbrace{\frac{\partial(\overline{2\nu'u_i'}S_{ij})}{\partial x_j}}^{\xi_{nn}}+\overbrace{\frac{\partial(\overline{2\nu's_{ij}'u_i'})}{\partial x_j}}^{\mathcal{D}_{nn}}\Bigg\}\overbrace{-\overline{2\nu's_{ij}'}S_{ij}}^{\chi_{nn}}\overbrace{-\overline{2\nu's_{ij}'s_{ij}'}}^{\epsilon_{nn}}=0. \tag{16}$$

The terms in the first row appear for both Newtonian and non-Newtonian fluids, for which the following is standard terminology:

$\mathcal{P}$**:** turbulent kinetic energy production;

$\mathcal{T}$**:** turbulent velocity transport;

Π**:** pressure related transport;

$\mathcal{D}$**:** mean viscous transport;

ϵ**:** mean viscous dissipation.

The terms in the second row in Eq. 16 appear due to viscosity fluctuations and therefore, vanish for Newtonian fluids. The following terminology is used for these terms:

ξ_{nn}**:** mean shear turbulent viscous transport;

$\mathcal{D}_{nn}$**:** turbulent viscous transport;

χ_{nn}**:** mean shear turbulent viscous dissipation;

ϵ_{nn}**:** turbulent viscous dissipation.

In the terminology used here, the nature of different terms (transport, production, dissipation etc.) has been identified in their name. The kinetic energy is generated via the productions terms, redistributed within the domain via the transport terms and dissipated via dissipation terms. The TKE production $\mathcal{P}$ appears in both equations with opposite sign and threfore, represents the kinetic energy transfer from the mean flow to turbulence. Note that the non-Newtonian terms χ_{nn}, ϵ_{nn} are named as dissipation terms due to their similarity with the Newtonian dissipation terms ϵ^m and ϵ. These non-Newtonian terms are not strictly dissipation terms and have been found to be positive for shear-thinning fluids and therefore, reduce the dissipation arising from the Newtonian terms[8]. The mean flow and turbulent kinetic energy budgets are discussed in detail in Davidson[32], Eggels[33] for Newtonian fluids and the effect of shear thinning for a fixed Re_τ is presented in Singh, Rudman, and Blackburn[8]. Here, the energy budgets are analysed to see whether the effect of shear thinning on the mean flow and the turbulent kinetic energy budgets is enhanced or diminished with increasing Re_τ.

B. Mean flow kinetic energy budget

The mean flow receives energy via the working of the mean pressure gradient on the mean flow and dissipates via viscous effects. Energy is transferred from the mean flow to TKE via production $\mathcal{P}^+$. For shear thinning, viscosity fluctuations introduce additional terms, the turbulent viscous stress transport Υ^m_{nn} and the mean shear turbulent viscous transport χ^+_{nn}. Since $\mathcal{P}^+$ and χ^+_{nn} appear in both MFKE and TKE budget equations, these terms are discussed later with the TKE budget and the remaining MFKE budget terms are plotted in Fig. 18 where the main points are discussed below.

The Newtonian MFKE budget terms, $W^+_{dp/dz}$, $\mathcal{T}^{m^+}$,$\mathcal{D}^{m^+}$ and ϵ^{m^+}, by definition depend on a mean shear stress component (τ^{v+}, τ^{R^+} or τ^{fv^+}) and mean axial velocity U_z^+. Therefore, similar to the mean axial velocity and the mean shear stresses, the Newtonian MFKE budget terms are affected similarly with Re_τ for both fluids. The MFKE production, $W^+_{dp/dz} = (U_z^+\partial P^+/\partial z^+)$ which can also be written as $2U_z^+/Re_\tau$, decreases with increasing Re_τ (Fig. 18 *a*). The turbulent transport of MFKE, $\mathcal{T}^{m^+}$, is a sink of MFKE in the core region where it balances the MFKE production (other MFKE budget terms vanish there). The location where $\mathcal{T}^{m^+}$ reaches a local maximum slightly shifts towards the wall with increasing Re_τ for both fluids. The magnitude of $\mathcal{T}^{m^+}$ decreases in the core region with increasing Re_τ, which is due to the lower MFKE production there for larger Re_τ. The turbulent transport $\mathcal{T}^{m^+}$ changes sign around $y^+ \approx 60$ and thus transports energy from the core region towards the wall. Similar to the axial turbulence intensity ($u_z'^+$) profiles, the profiles of $\mathcal{T}^{m^+}$ of Newtonian and PL fluids overlap each other in the core region, however, there is no obvious relation between $\mathcal{T}^{m^+}$ and $u_z'^+$.

The remaining terms are the viscosity dependent terms ($\mathcal{D}^{m^+}$, ϵ^{m^+} and Υ^+_{nn}) which are significant only near the wall for $y^+ \lesssim 100$ (Fig. 18 *c*–*e*). The mean viscosity dependent terms i.e. the mean viscous transport, $\mathcal{D}^{m^+}$, and the mean viscous dissipation, ϵ^{m^+}, dominate the MFKE budget near the wall and similar to the mean viscous stress, τ^{v^+}, both of these terms show a marginal dependence on Re_τ. Due to the higher τ^{v^+} in the shear-thinning fluid, the magnitude of $\mathcal{D}^{m^+}$ and ϵ_{m^+} is higher for PL fluid compared to the Newtonian fluid. The turbulent viscous stress transport, Υ^+_{nn}, which is due to

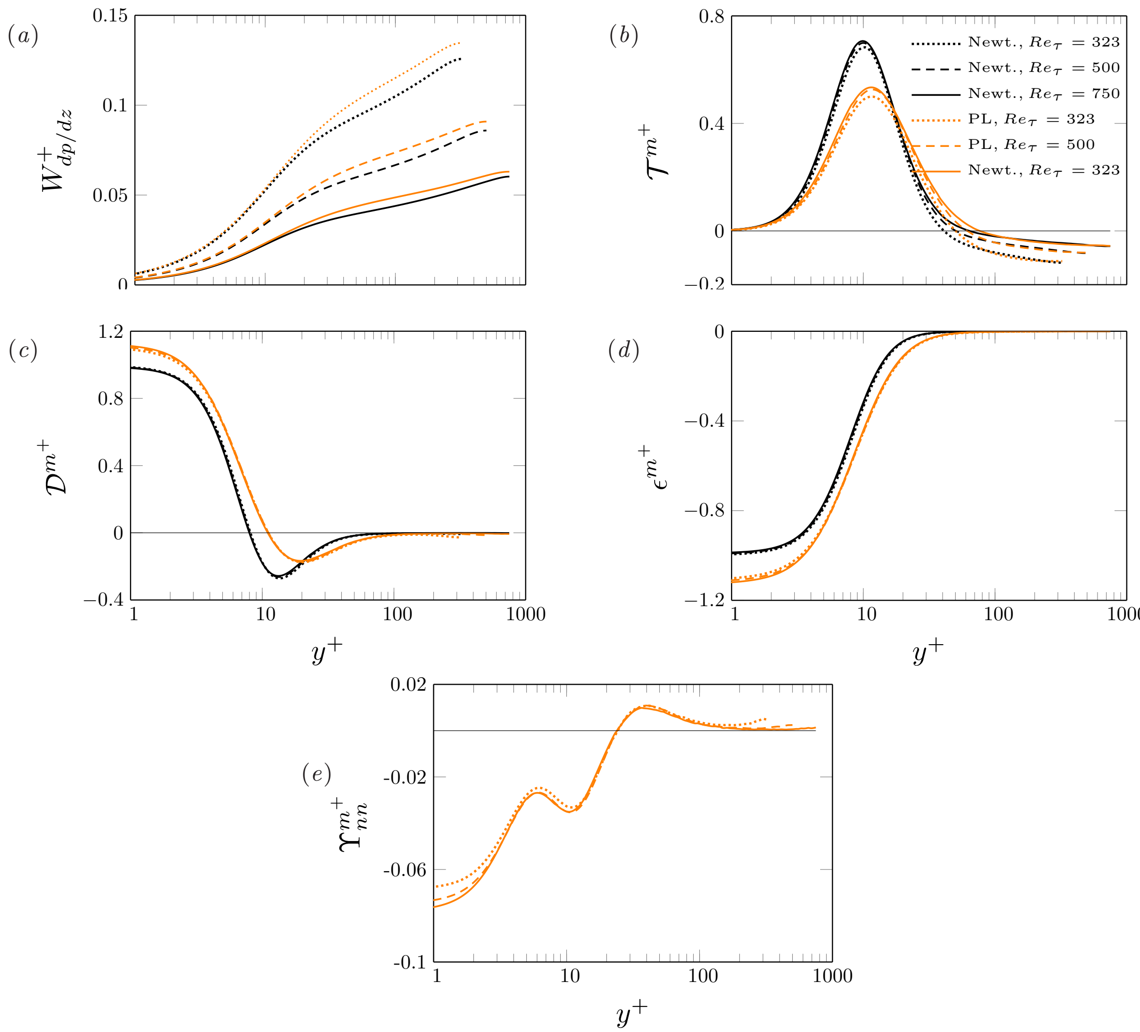

FIG. 18. Profiles of the terms which appear only in the mean flow kinetic energy budget (Eq. 15) plotted for Newtonian (black lines) and PL fluids (orange lines).

the turbulent viscous stress τ^{fv^+}, show a similar Re_τ-dependence as seen for τ^{fv^+} in Fig. 15 (c) and slightly increases with increasing Re_τ. However, the magnitude of Υ^+_{nn} is very small compared to the mean viscous dissipation ϵ^{m^+}. The negative values Υ^+_{nn} close to the wall suggest that it decreases the total viscous dissipation there.

Overall, the Reynolds number dependence of the MFKE budget terms is similar for both the fluids and the contribution of the non-Newtonian transport term, Υ^+_{nn}, is small in the total MFKE transport.

C. Turbulent kinetic energy budget

As mentioned earlier, TKE receives energy from the mean flow via the TKE production $\mathcal{P}^+$ and similar to the MFKE, TKE is dissipated via the viscous effects. Viscosity fluctuations introduce additional transport (ξ_{nn}, $\mathcal{D}_{nn}$) and dissipation (χ_{nn} and ϵ_{nn}) terms. Profiles of different TKE budget terms are plotted in Fig. 19 where the main points are discussed below.

Similar to the MFKE budget, Newtonian terms in the TKE budget are also similarly affected by increasing Re_τ for each fluid (Fig. 19 a-e). The TKE production, $\mathcal{P}^+ = \tau^{R^+}(\partial U_z^+/\partial y^+)$, is higher for higher Re_τ for each fluid (Fig. 19 a), which is due to the increased Reynolds shear stress τ^{R^+} with increasing Re_τ as seen in Fig. 15 (c). The location of the maximum $\mathcal{P}^+$ is almost indpendent of Re_τ but slightly shifts away from the wall with shear thinning. Shear thinning decreases τ^{R^+}, therefore, the TKE production $\mathcal{P}^+$ is lower for PL compared to the Newtonian fluid. The gap between $\mathcal{P}^+$ profiles of Newtonian and PL fluids is significantly large at all Re_τ.

The increase in the TKE production with increasing Re_τ is accompanied by an increase in the mean viscous dissipation, ϵ^+ (Fig. 19 b). The mean viscous dissipation

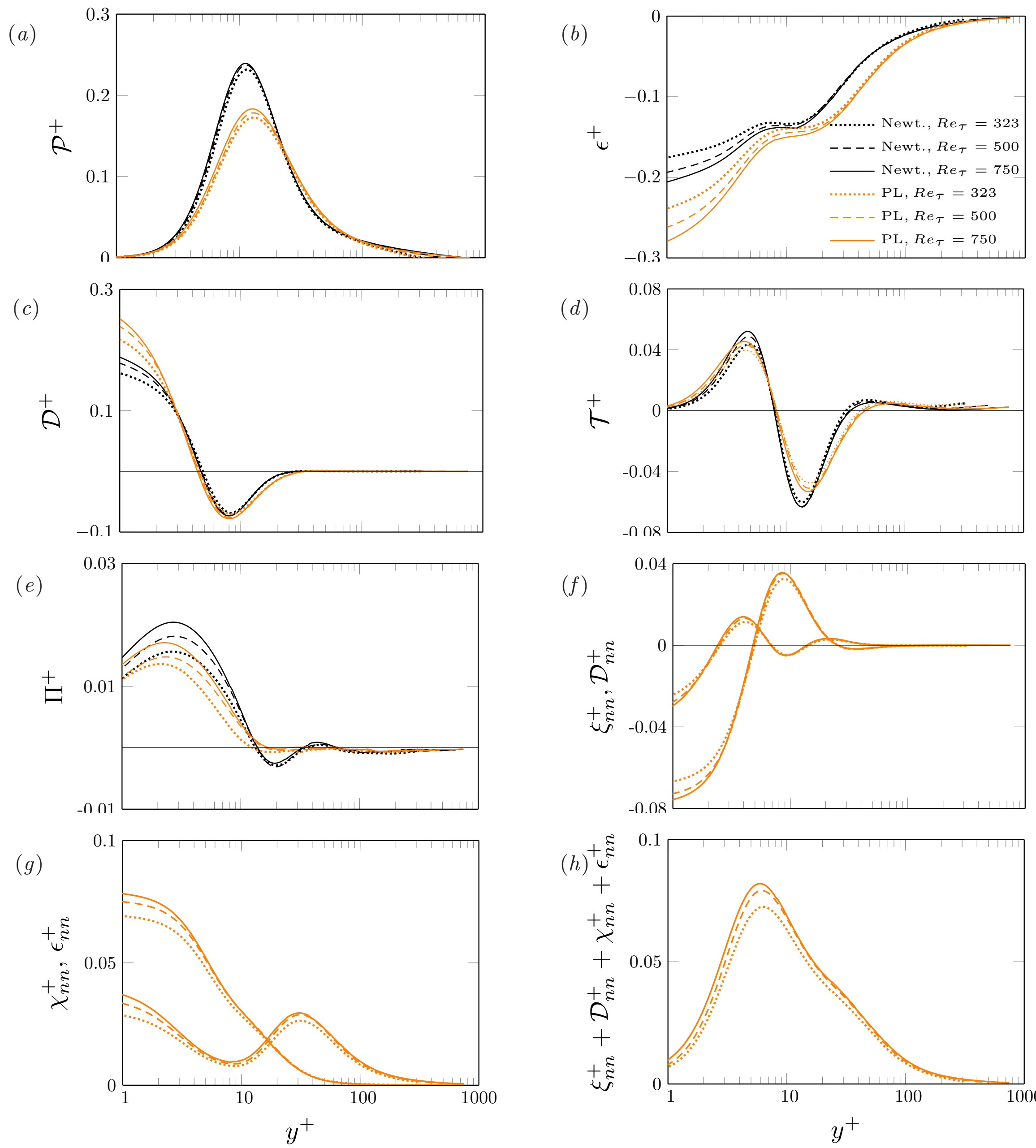

FIG. 19. Profiles of the turbulent kinetic energy budget terms (see Eq. 16) plotted for Newtonian (black lines) and PL fluids (orange lines) at different Re_τ.

ϵ^+ shows Re_τ-dependence mainly for $y^+ \lesssim 30$. Larger ϵ^+ near the wall for higher Re_τ indicates larger shear rate fluctuations $\overline{s'_{ij}s'_{ij}}^+$ ($\epsilon^+ = 2\nu^+\overline{s'_{ij}s'_{ij}}^+$) for higher Re_τ because the mean viscosity is constant for a Newtonian fluid and is independent of Re_τ there for PL fluid (Fig. 12). Deviation between the profiles of Newtonian and PL fluids in the viscous sublayer slightly increases with increasing Re_τ.

The mean viscous dissipation near the wall is mainly balanced by the mean viscous transport, $\mathcal{D}^+$, there. Therefore, the profiles of $\mathcal{D}^+$ show a similar Re_τ-dependence as ϵ^+ for $y^+ < 3$, and $\mathcal{D}^+$ there is larger for higher Re_τ (figure 19 *c*). The mean viscous transport $\mathcal{D}^+$ vanishes beyond $y^+ \gtrsim 30$. Profiles of the other Newtonian transport terms, $\mathcal{T}^+$ and Π^+, which are small compared to $\mathcal{D}^+$ (approximately five and ten times smaller), also show a similar Re_τ-dependence for each fluid as seen for the mean viscous transport $\mathcal{D}^+$ (figures 19 *d* and *e*). However unlike $\mathcal{D}^+$, $\mathcal{T}^+$ and Π^+ do not vanish until $y^+ \approx 100$. The non-Newtonian terms arising due to viscosity fluctuations are significant only for $y^+ \lesssim 30$ where

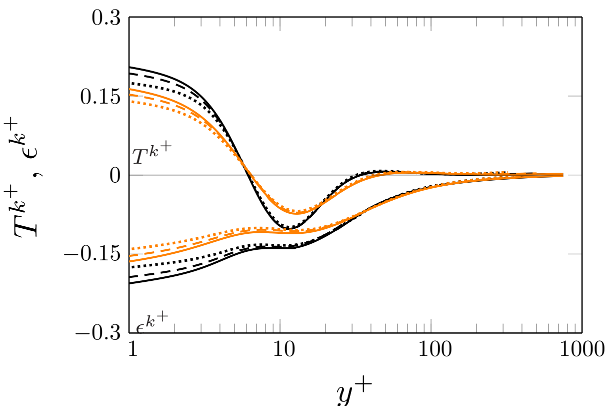

FIG. 20. Profiles of the sum of the Newtonian and non-Newtonian transport and the dissipation terms plotted for the Newtonian (black lines) and the shear-thinning fluid (orange lines).

they increase in magnitude with increasing Re_τ (figures 19 *f* and *g*).

Profiles of the total transport $T^{k^+} = \mathcal{T}^+ + \Pi^+ + \mathcal{D}^+ + \xi^+_{nn} + \mathcal{D}^+_{nn}$ and the total dissipation $\epsilon^{k^+} = \epsilon^+ + \chi^+_{nn} + \epsilon^+_{nn}$ provide a complete picture of the effect of increasing Re_τ on the turbulent kinetic energy budget. As seen in Fig. 20 the profiles of both T^{k^+} and ϵ^{k^+} are also affected similarly with increasing Re_τ for each fluid. Both T^{k^+} and ϵ_{k^+} are larger for higher Re_τ. The total TKE transport, T^{k^+}, shows a Re_τ-dependence only in the viscous sublayer whereas the total turbulence dissipation ϵ^{k^+} is affected by increasing Re_τ until the outer edge of the buffer layer ($y^+ \lesssim 30$). The gap between the profiles of Newtonian and PL fluids is larger in the viscous sublayer and it seems unlikely that the gap will close even at very high Reynolds number.

The overall effect of increasing Re_τ on the TKE budget is qualitatively similar for each fluid. The non-Newtonian terms act as a sink in the TKE budget and their contribution increases with increasing Re_τ. The Reynolds number effect is mainly confined near the wall for $y^+ \lesssim 30$ whereas the shear-thinning effect is seen until $y^+ \approx 100$. The shear-thinning effect on the energy budgets is unlikely to disappear even at very high Reynolds number.